Inorganica Chimica Acta, 37 (1979) 169–179

The High-spin($^5T_2$) ⇌ Low-spin($^1A_1$) Transition in Solid Dithiocyanatobis(2,2'-bi-2-thiazoline)iron(II). Hysteresis Effects, Debye–Waller Factors and Crystallographic Changes

E. KÖNIG,* G. RITTER, W. IRLER

Institut für Physikalische und Theoretische Chemie and Physikalisches Institut, Abt. II, Universität Erlangen-Nürnberg, D-8520 Erlangen, F.R.G.

and S. M. NELSON

Department of Chemistry, Queen's University, Belfast BT9 5AG, U.K.

Received February 13, 1979

The almost discontinuous high-spin($^5T_2$) ⇌ low-spin($^1A_1$) transition in solid [Fe(bt)$_2$(NCS)$_2$] (bt = 2,2'-bi-2-thiazoline) has been studied in detail by ^{57}Fe Mössbauer spectroscopy and X-ray diffraction. At the transition temperature T_c, the ground states involved are characterized by $\Delta E_Q(^5T_2)$ = 3.00 mm s^{-1}, $\delta^{IS}(^5T_2)$ = +0.97 mm s^{-1} and $\Delta E_Q(^1A_1)$ = 0.54 mm s^{-1}, $\delta^{IS}(^1A_1)$ = +0.30 mm s^{-1}. A pronounced hysteresis of ΔT_c = 9.5 K has been observed, the transition being centred on $T_c^{>}$ = 181.86 K for rising and on $T_c^{<}$ = 172.33 K for falling temperatures. The observations are compared with a Bragg and Williams type theory and with the independent domain model. Debye–Waller factors show at T_c a discontinuity of $\Delta f_{total} \sim 35.4\%$ corresponding to the change between $-\ln f_{^5T_2}$ and $-\ln f_{^1A_1}$. The X-ray diffraction patterns for the $^5T_2$ and $^1A_1$ phases show characteristic differences. The temperature dependence for $t_{^5T_2}/t_{total}$ of the Mössbauer effect and for the relative intensities $I_{^5T_2}/I_{total}$ of individual peak profiles of X-ray diffraction is equivalent. The observations provide evidence for a crystallographic phase change which is associated with the (S = 2) ⇌ (S = 0) spin transformation. The existence of crystal domains of finite dimension is required for both $^5T_2$ and $^1A_1$ ground state molecules.

Introduction

High-spin($^5T_2$) ⇌ low-spin($^1A_1$) transitions of a more or less discontinuous type have been observed in a number of systems of [Fe^{II}-N$_6$] type, *e.g.* [Fe(phen)$_2$(NCS)$_2$] and [Fe(phen)$_2$(NCSe)$_2$] where phen = 1,10-phenanthroline [1]. More details on high-spin($^5T_2$) ⇌ low-spin($^1A_1$) transitions which may be useful as an introduction into the field may be found elsewhere [2–4]. The first-order character of the transitions has been established, on a thermodynamic basis, by the entropy change determined as ΔS = 48.78 J K^{-1} mol^{-1} and ΔS = 51.22 J K^{-1} mol^{-1}, at the transition temperature, for the NCS- and the NCSe-compound, respectively [5]. On the other hand, application of the Frenkel theory of heterophase fluctuations in liquids [6] produced, as characteristic parameters, the number of cells, N = 6.34 × 10^{21} mol^{-1} and N = 7.83 × 10^{21} mol^{-1}, and the number of molecules per cell, n = 95 and n = 77, for the NCS- and NCSe-complex, serially. Here, a reduction of the first-order character of the transition is reflected, within the applied model, in the large value for N.

The hysteresis phenomenon is equally indicative of the first-order character of a transition. For the above two compounds, $\Delta H = T\Delta S$ is closely followed and thus hysteresis is not expected. Although hysteresis effects may be quite common in discontinuous high-spin($^5T_2$) ⇌ low-spin($^1A_1$) transitions, it seems that only in [Fe(4,7-(CH$_3$)$_2$-phen)$_2$(NCS)$_2$] the hysteresis has been investigated in some detail [7].

A discontinuity in the Debye–Waller factor provides evidence for an anomalous change of the lattice dynamical properties which is often associated with a phase transformation. For [Fe(4,7-(CH$_3$)$_2$-phen)$_2$(NCS)$_2$], a well defined discontinuity of $\Delta f_{total} \sim 20\%$ has been found at T_c = 121.5 K [8] which corresponds to the change between $-\ln f_{^5T_2}$ and $-\ln f_{^1A_1}$.

Although the most direct information on a phase transformation is usually obtained from X-ray structure data, there have been very few reports on such studies in high-spin($^5T_2$) ⇌ low-spin($^1A_1$) systems which were performed both above and below the transition temperature, T_c [9, 10]. Even if spin

*Author to whom correspondence should be addressed.

transitions in all possible configurations are taken into account, the number of such studies remains strictly limited [9–12]. In particular, investigations of X-ray diffraction over a more extended range of temperature have not been attempted.

Recently, one of the present authors reported the synthesis of a series of iron(II) complexes of the type $[FeL_2X_2]$ where L denotes a bidentate NN ligand and X = NCS, NCSe [13]. Some of these compounds exhibit discontinuous high-spin($^5T_2$) ⇌ low-spin($^1A_1$) transitions with T_c between 170 and 210 K. The object of the present work is the more detailed investigation of the hysteresis, Debye–Waller factors and X-ray diffraction employing, as a representative example, the compound $[Fe(bt)_2(NCS)_2]$ where bt = 2,2′-bi-2-thiazoline, $C_6H_8N_2S_2$, *i.e.*

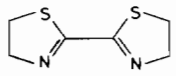

Experimental

Samples of $[Fe(bt)_2(NCS)_2]$ were prepared as described elsewhere [13], the homogeneity and purity of the products being verified by chemical analyses, optical and IR spectra, magnetism and the physical properties reported below.

^{57}Fe Mössbauer spectra were measured with a spectrometer of the constant-acceleration type (Elscint AME-30A) operating in the multiscaler mode. A 50-mCi source of ^{57}Co in rhodium was used, the calibration being effected with a metallic-iron absorber. All velocity scales and isomer shifts are referred to the iron standard at 298 K. To convert to the sodium nitroprusside scale, add +0.257 mm s^{-1}. Movement of the source toward the absorber corresponds to positive velocities. Variable-temperature measurements between 12 and 304 K were obtained by the use of a closed-cycle refrigerator (Air Products Displex Type CSA-202C) and a suitable cryostat (Air Products DMX-20). The temperatures were monitored by means of a calibrated gold–iron *vs.* chromel thermocouple and a cryogenic temperature controller (Air Products Type APD-C1). All measurements were performed with the identical geometrical arrangement for source, absorber, and detector. The resulting data were carefully corrected for non-resonant background of the γ rays, and the individual areas $A(^5T_2)$ and $A(^1A_1)$ were extracted by a computer-based decomposition into Lorentzians.

To obtain values for the effective thickness $t_{^5T_2}$ and $t_{^1A_1}$, the well-known area method [14, 15] has been utilized. Following this procedure, the normalized area [15] for the i-th line is determined, assuming an absorber of finite thickness, by

$$A_i = \frac{1}{2}\pi f_S \Gamma_i L(t_i) \qquad (1)$$

Here, Γ_i is the line width of the i-th absorber line (in the present case, $\Gamma_i = \Gamma_0$ where Γ_0 is the natural line width), f_S is the Debye–Waller factor of the source, and $L(t_i)$ the saturation function. In order to determine, from the quantity A_i of eqn. (1), the effective thickness t_i, the inverse function to $L(t_i)$ is required. This function is given for $0 \leqslant t_i \leqslant 2$ by

$$t_i(L) = L(t_i)/[1 - \tfrac{1}{4} L(t_i)] \qquad (2)$$

with an accuracy of better than 1%. The effective thickness for a single line of the quadrupole doublet in the appropriate solid phase is then determined according to

$$t_{^5T_2} = \tfrac{1}{2} N\beta d\sigma_0 f_{^5T_2} n_{^5T_2}$$
$$t_{^1A_1} = \tfrac{1}{2} N\beta d\sigma_0 f_{^1A_1}(1 - n_{^5T_2}) \qquad (3)$$

In eqn. (3), N is the number of iron atoms per unit volume, β the isotopic abundance, d the absorber thickness, and σ_0 the resonance cross-section. In addition, $f_{^5T_2}$ and $f_{^1A_1}$ are the Debye–Waller factors for the $^5T_2$ and $^1A_1$ phase, respectively, and $n_{^5T_2}$ is the site fraction of the corresponding molecules.

In most systems showing a high-spin($^5T_2$) ⇌ low-spin($^1A_1$) transition, the determination of $n_{^5T_2}$ is rather intricate, and recourse to the results of an independent physical measurement has usually been taken [16–19]. In the present system, the contribution to the total area, A_{total}, outside the transition region (*i.e.* at the temperatures $T \gtrsim T_c + 4$ K and $T \lesssim T_c - 4$ K) by the $^1A_1$ and $^5T_2$ phase, respectively, is negligible, *cf.* Fig. 1. Consequently, we may assume to first approximation

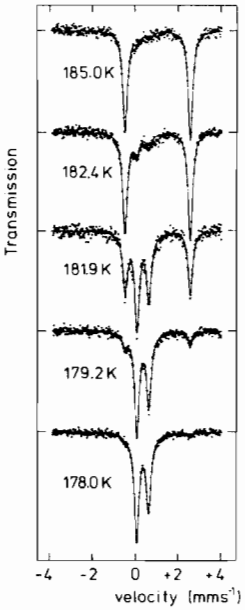

Fig. 1. ^{57}Fe Mössbauer spectra of $[Fe(bt)_2(NCS)_2]$ collected for increasing temperatures at 178.0, 179.2, 181.9 ($T_c^{\gtrless}$), 182.4 and 185.0 K.

$$f_{^5T_2} = f_{total} \text{ for } T \gtrsim T_c + 4\ K$$
$$f_{^1A_1} = f_{total} \text{ for } T \lesssim T_c - 4\ K \quad (4)$$

The factor $\frac{1}{2}\pi f_S \Gamma_0$ has been determined by measurements on thin absorbers of sodium nitroprusside. The Debye–Waller factors then follow from the application of eqn. (1) through eqn. (4) to the data of A_{total}. It should be observed that, because of the difference between $f_{^5T_2}$ and $f_{^1A_1}$, an observed variation in $t_{^5T_2}$ and $t_{^1A_1}$ will not directly reflect the variation in $n_{^5T_2}$ and $n_{^1A_1} = 1 - n_{^5T_2}$, respectively. Therefore, in the hysteresis study, the relative effective thickness for the $^5T_2$ phase, *viz.* $t_{^5T_2}/(t_{^5T_2} + t_{^1A_1})$, has been employed.

In order to determine scanning curves, a more accurate control of temperature than that provided by the closed-cycle refrigerator is required. Therefore, the temperature was monitored with an Artronix Model 5301-E cryogenic controller using a small heating coil and liquid nitrogen as coolant, the sample being placed in a specially designed superinsulated cryostat. With a calibrated copper *vs.* constantan thermocouple a relative accuracy of about 0.05 K was achieved, the absolute accuracy of the temperatures being about ±0.5 K.

Measurements of X-ray powder diffraction were performed with a Siemens counter diffractometer equipped with an Oxford Instruments CF 108A cryostat. CuK_α radiation was used throughout. Measurements of peak profiles were carried out in the mode of step scanning of the apparatus, the resulting pulses being stored and processed by a multichannel analyzer (Elscint MEDA 10). The smallest steps which the available equipment produces amount to 0.005° in 2θ. The resulting angular resolution was required in order to observe the changes reported below, *cf.* also Fig. 6. The individual peaks were fitted to Gaussian line shape on a PDP-11 computer. The relative accuracy of the temperature reading is about 0.1 K, whereas the absolute accuracy is not better than ±3.0 K. Discrepancies between temperature listings for Mössbauer effect and X-ray diffraction measurements are due to the use of different temperature control equipment. Obviously, the simultaneous calibration of the two experimental setups is difficult to achieve.

Results

(i) Temperature Dependence of ^{57}Fe Mössbauer Spectra

The ^{57}Fe Mössbauer spectrum of the solid complex $[Fe(bt)_2(NCS)_2]$ was measured between 12.2 and 302.0 K. At the lowest temperature studied, *i.e.* 12.2 K, a single doublet characterized by the quadrupole splitting $\Delta E_Q = 0.55 \pm 0.01$ mm s^{-1} and the isomer shift $\delta^{IS} = +0.26 \pm 0.03$ mm s^{-1} is observed. On the basis of these data, in conjunction with the results of magnetic measurements [13], assignment of the doublet to the low-spin $^1A_1(t_2^6)$ ground state is justified. Term symbols of cubic symmetry are employed for convenience only. Up to and inclusive of 177.0 K, the Mössbauer spectra are essentially identical to that at 12.2 K, the values of ΔE_Q and δ^{IS} remaining constant, within experimental uncertainty (*cf.* Table I), as expected. At 179.2 K,

TABLE I. ^{57}Fe Mössbauer Effect Data for the Low-spin($^1A_1$) Ground State of $[Fe(bt)_2(NCS)_2]$.

T (K)	$\Delta E_Q(^1A_1)$[a] (mm s^{-1})	$\delta^{IS}(^1A_1)$[b,c] (mm s^{-1})	$-\ln f_{^1A_1}$[d]
12.2	0.55	+0.26	0.51
21.0	0.55	+0.26	0.52
32.0	0.55	+0.26	0.55
41.9	0.56	+0.26	0.57
51.5	0.55	+0.26	0.62
62.9	0.55	+0.27	0.65
71.5	0.55	+0.27	0.68
85.4	0.54	+0.27	0.73
96.8	0.54	+0.27	0.79
108.8	0.54	+0.28	0.85
119.2	0.55	+0.28	0.89
128.3	0.56	+0.28	0.94
138.8	0.56	+0.29	0.99
155.8	0.55	+0.29	1.09
166.0	0.55	+0.30	1.16
172.9	0.55	+0.30	1.22
177.0	0.55	+0.30	1.23
180.0	0.54	+0.30	1.25

[a]Experimental uncertainty of ΔE_Q is ±0.01 mm s^{-1}. [b]Experimental uncertainty of δ^{IS} is ±0.03 mm s^{-1}. [c]Isomer shifts δ^{IS} are listed relative to natural iron at 298 K. [d]Standard deviation of $-\ln f_{^1A_1}$ is ±0.02.

a second weak doublet (~18.0%) becomes visible. On the basis of its Mössbauer parameters, *viz.* $\Delta E_Q = 2.99 \pm 0.03$ mm s^{-1}, $\delta^{IS} = +0.98 \pm 0.05$ mm s^{-1}, this doublet is assigned to the high-spin ground state $^5T_2$-$(t_2^4e^2)$. The intensity of the $^5T_2$ doublet increases rapidly with increasing temperature, the intensity of the $^1A_1$ spectrum decreasing at the same rate, *cf.* Fig. 1. Already at 185.0 K, the spectrum is for the larger part (*i.e.* ~94.0%) due to the $^5T_2$ doublet, the corresponding Mössbauer parameters being determined as $\Delta E_Q = 3.00 \pm 0.01$ mm s^{-1}, $\delta^{IS} = +0.97 \pm 0.02$ mm s^{-1}. With further increase of temperature the Mössbauer spectrum consists only of the $^5T_2$ doublet, the values of ΔE_Q slowly decreasing in magnitude (*cf.* Table II) until, at 302.0 K, $\Delta E_Q = 2.70 \pm 0.01$ mm s^{-1}. The high-spin($^5T_2$) ⇌ low-spin($^1A_1$) transition in $[Fe(bt)_2(NCS)_2]$ is thus completed within a very narrow temperature range. This observation which is in complete agreement with the magnetic data [13] is considerable evidence that a phase transition is

TABLE II. ^{57}Fe Mössbauer Effect Data for the High-spin-($^5T_2$) Ground State of $[Fe(bt)_2(NCS)_2]$.

T (K)	$\Delta E_Q(^5T_2)$[a] (mm s^{-1})	$\delta^{IS}(^5T_2)$[b,c] (mm s^{-1})	$-\ln f_{^5T_2}$[d]
185.0	3.00	+0.97	1.72
194.9	2.99	+0.97	1.72
195.9	2.99	+0.97	1.80
217.1	2.95	+0.97	1.98
230.4	2.91	+0.98	2.12
252.0	2.85	+0.98	2.34
261.5	2.82	+0.97	2.43
278.5	2.77	+0.97	2.63
302.0	2.70	+0.96	2.85

[a]Experimental uncertainty of ΔE_Q is ±0.01 mm s^{-1}. [b]Experimental uncertainty of δ^{IS} is ±0.02 mm s^{-1}. [c]Isomer shifts δ^{IS} are listed relative to natural iron at 298 K. [d]Standard deviation of $-\ln f_{^5T_2}$ is ±0.015.

involved. The transition temperature may be estimated (*vide infra*), for increasing temperatures, *i.e.* for the process $^1A_1 \rightarrow {}^5T_2$, at $T_c^{>} = 181.9$ K. If the temperature is decreased, starting from 302.0 K, spectra which are similar, on a qualitative basis, to those discussed above are obtained in reversed order. If now, within the transition region, spectra for the same temperature are compared, considerably different relative intensities for the $^1A_1$ and $^5T_2$ doublets are found. This is an indication that hysteresis effects are operative and indeed $T_c^{<} = 172.5$ K may be obtained for the process $^5T_2 \rightarrow {}^1A_1$ as will be shown in section 3.2.

(ii) Experimental Study of Hysteresis

The hysteresis associated with the high-spin($^5T_2$) ⇌ low-spin($^1A_1$) transition in $[Fe(bt)_2(NCS)_2]$ is illustrated by Fig. 2. Here, the relative effective thickness $t_{^5T_2}/t_{total}$ extracted from the Mössbauer spectra has been plotted as the internal dependent variable versus temperature as the external independent variable. Figure 2 shows the results for two specific temperature cycles within the immediate neighborhood of T_c. Starting at 167.0 K, the temperature has been gradually increased up to 185.0 K as indicated by the rising arrows. By this process, the first branch of the hysteresis loop is obtained. If now the temperature is lowered gradually as indicated by the falling arrows, the starting value of temperature will be eventually reached and thus the second branch of the hysteresis loop forms. The detailed values of $t_{^5T_2}/(t_{^5T_2} + t_{^1A_1})$ are presented in Table III. A transition temperature T_c may now be defined as that temperature at which $n_{^5T_2} = 0.50$. Accordingly, the observed transition is centred, for increasing temperatures, on $T_c^{>} = 181.91$ K, whereas for decreasing temperatures, $T_c^{<} = 172.54$ K, *cf.* Fig. 2. This estimate is based on the assumption of equal Debye–Waller factors, *i.e.* $t_{^5T_2}/t_{total} = n_{^5T_2}$. If corrections for differences in $f_{^5T_2}$ and $f_{^1A_1}$ (*cf.* section 3.4) are applied, the more precise values $T_c^{>} = 181.86$ K and $T_c^{<} = 172.33$ K are obtained.

In order to produce a scanning curve, the temperature rise in the first branch has been interrupted at 182.07 K ($t_{^5T_2}/t_{total} = 0.594$), and the temperature has been gradually lowered to 172.25 K ($t_{^5T_2}/t_{total} = 0.241$). If the temperature is subsequently increased to 182.30 K ($t_{^5T_2}/t_{total} = 0.755$), the inner loop of

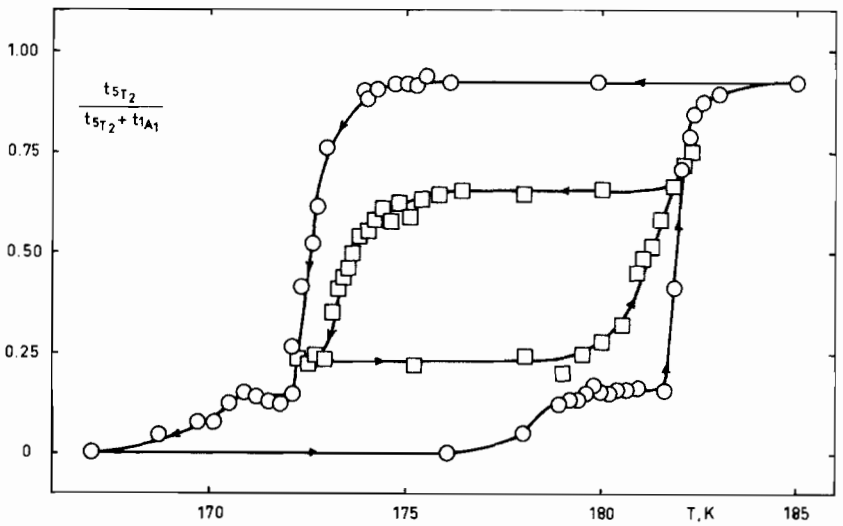

Fig. 2. Temperature dependence of the relative effective thickness $t_{^5T_2}/(t_{^5T_2} + t_{^1A_1})$ for $[Fe(bt)_2(NCS)_2]$ in the immediate neighborhood of T_c. Rising arrows indicate increase of temperature, falling arrows indicate decrease of temperature. The centers for the two branches of the hysteresis loop are found at $T_c^{>} = 181.86$ K and $T_c^{<} = 172.54$ K.

TABLE III. The Relative Effective Thickness $t_{s_{T_2}}/(t_{s_{T_2}} + t_{1_{A_1}})$ and the High-spin Fraction $n_{s_{T_2}}$ for the Main Branches of the Hysteresis Loop in $[Fe(bt)_2(NCS)_2]$.

T (K)	$\frac{t_{s_{T_2}}}{t_{s_{T_2}} + t_{1_{A_1}}}$	$n_{s_{T_2}}$
167.00	0	0
176.00	0	0
178.00	0.053	0.074
178.90	0.124	0.168
179.20	0.134	0.181
179.40	0.132	0.179
179.60	0.150	0.202
179.80	0.169	0.226
180.00	0.157	0.211
180.20	0.151	0.203
180.40	0.161	0.216
180.65	0.160	0.215
180.95	0.165	0.221
181.60	0.157	0.212
181.86	0.413	0.504
182.03	0.708	0.778
182.25	0.789	0.844
182.35	0.845	0.887
182.60	0.873	0.909
183.00	0.895	0.925
185.00	0.920	0.944
179.90	0.925	0.947
176.10	0.922	0.944
175.50	0.940	0.957
175.25	0.916	0.939
175.00	0.920	0.942
174.70	0.917	0.940
174.25	0.905	0.931
173.90	0.900	0.927
173.70	0.890	0.919
172.70	0.770	0.824
172.40	0.623	0.698
172.33	0.414	0.497
172.10	0.150	0.198
171.80	0.124	0.165
171.50	0.131	0.174
171.20	0.143	0.189
170.90	0.152	0.200
170.50	0.125	0.166
170.10	0.077	0.104
169.70	0.079	0.106
168.70	0.047	0.064
167.00	0	0

Fig. 2 is completed. It has been verified that the obtained scanning curve as well as the main branches of the hysteresis loop are stable and reproducible as required.

A more detailed inspection of Fig. 2 shows that the shapes of the two branches of the hysteresis loop are slightly different, the rising branch being steeper than the falling branch. A similar observation has been made for the hysteresis loop of $[Fe(4,7\text{-}(CH_3)_2\text{-}phen)_2(NCS)_2]$ [8]. It will be also noticed that the transition seems to be preceeded, for rising temperatures, and succeeded, for falling temperatures, by a second though less prominent transition. This peculiarity has been disregarded in the present discussion, since it will be shown in section 3.6 below that, most likely, it is due to the presence of another modification of $[Fe(bt)_2(NCS)_2]$.

(iii) Model Calculations

If, for the transformation $^1A_1 \rightarrow {}^5T_2$ the transition temperature $T_c^{>} = T_c(^1A_1 \rightarrow {}^5T_2)$ is approached, some $^5T_2$ systems will be formed within the $^1A_1$ phase at the expense of $^1A_1$ systems. The opposite process will take place at $T_c^{<} = T_c(^5T_2 \rightarrow {}^1A_1)$ for the transformation in the reverse direction, *i.e.* $^5T_2 \rightarrow {}^1A_1$. Close to the transition point, the Gibbs free energy for the total system may be written as [20, 21]

$$G = N_0[(1 - n_{s_{T_2}})G_{1_{A_1}} + n_{s_{T_2}} G_{s_{T_2}} + n_{s_{T_2}}(1 - n_{s_{T_2}})\Gamma] + kTN_0[n_{s_{T_2}} \ln n_{s_{T_2}} + (1 - n_{s_{T_2}}) \ln (1 - n_{s_{T_2}})] \quad (5)$$

Here $n_{s_{T_2}}$ is the fraction of $^5T_2$ molecules, N_0 the total number of molecules per cubic centimeter, and Γ the net interaction energy between the $^1A_1$ and $^5T_2$ systems. Also, the last term in eqn. (5) is the mixing entropy contribution. If the system is in equilibrium, G is a minimum

$$\left(\frac{\partial G}{\partial n_{s_{T_2}}}\right)_{p,T} = 0 \quad (6)$$

and, consequently, the relation

$$G_{s_{T_2}} - G_{1_{A_1}} + (1 - 2n_{s_{T_2}})\Gamma + kT \ln[n_{s_{T_2}}/(1 - n_{s_{T_2}})] = 0 \quad (7)$$

is obtained. This result may be recast into the form

$$\ln[(1 - n_{s_{T_2}})/n_{s_{T_2}}] = \frac{\Delta H + (1 - 2n_{s_{T_2}})\Gamma}{kT} - \frac{\Delta S}{k} \quad (8)$$

which equation may be conveniently solved by graphical methods. The macroscopic thermodynamic model represented by eqn. (5) is well known in the area of liquid and solid mixtures [22, 23]. In the field of magnetism, eqn. (7) corresponds to the molecular field theory. In the present context we apply the model to the hysteresis associated with the high-spin($^5T_2$) $\rightleftharpoons$ low-spin($^1A_1$) transition in $[Fe(bt)_2(NCS)_2]$.

The solutions, $n_{s_{T_2}}$, to eqn. (8) are defined by the points of intersection, if the two sides of the equation are plotted separately as functions of $n_{s_{T_2}}$. Whereas an S-shaped curve is formed by the left hand side of

eqn. (8), the right hand side consists of a straight line through the point $[\frac{1}{2} + (\Delta H/2\Gamma), -\Delta S/k]$. In this model, hysteresis is observed if two straight lines can be constructed (for two different temperatures) which are tangents to the two branches of the S-shaped curve, *viz.* $\ln [(1 - n_{s_{T_2}})/n_{s_{T_2}}] > 0$ and $\ln [(1 - n_{s_{T_2}})/n_{s_{T_2}}] < 0$, respectively. The iterative solution for the experimentally determined temperatures $T_c^>$ and $T_c^<$ produces, as parameters of the model, values for the quantities ΔS and Γ.

Figure 3 illustrates an attempt to obtain a fit of the observed hysteresis loop on the basis of the model. The interaction energy results as $\Gamma/k = 446$, 476, and 503 K for $\Delta S = 50.0$, 75.0, and 100.0 J K^{-1} mol^{-1}, serially. These values are of reasonable magnitude (*viz.* $\Gamma = 310$ cm^{-1} for $\Delta S = 50.0$ J K^{-1} mol^{-1}), although in view of recent calorimetric results for two related compounds [5], the result for $\Delta S = 50.0$ J K^{-1} mol^{-1} is likely to be the most realistic one. It should be noticed that, in Fig. 3, the experimental points around $n_{s_{T_2}} = 0.15$ should be disregarded for the reasons mentioned at the end of the previous section.

If, according to the domain model [24–26], the present system is considered as an assembly of independent domains, the values of the transition temper-

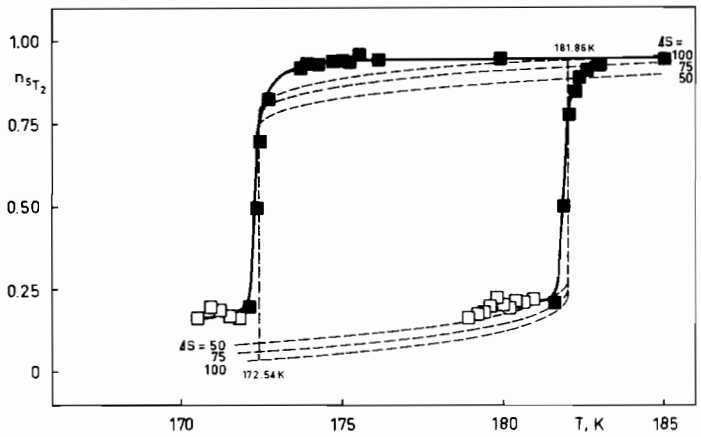

Fig. 3. Comparison of experimentally determined and calculated dependence of $n_{s_{T_2}}$ on temperature in the neighborhood of T_c: experimental data, full squares, full line; calculated curves, broken lines. Temperatures $T_c^>$ and $T_c^<$ as in Fig. 2, assumed entropy changes are $\Delta S = 50.0$, 75.0 and 100.0 J K^{-1} mol^{-1}. Open squares refer to experimental data which are most likely due to an additional modification. Neglect of these data causes the hysteresis loop to extend below the $\Delta S = 100.0$ J K^{-1} mol^{-1} curve, arriving for low temperatures at $n_{s_{T_2}} = 0$.

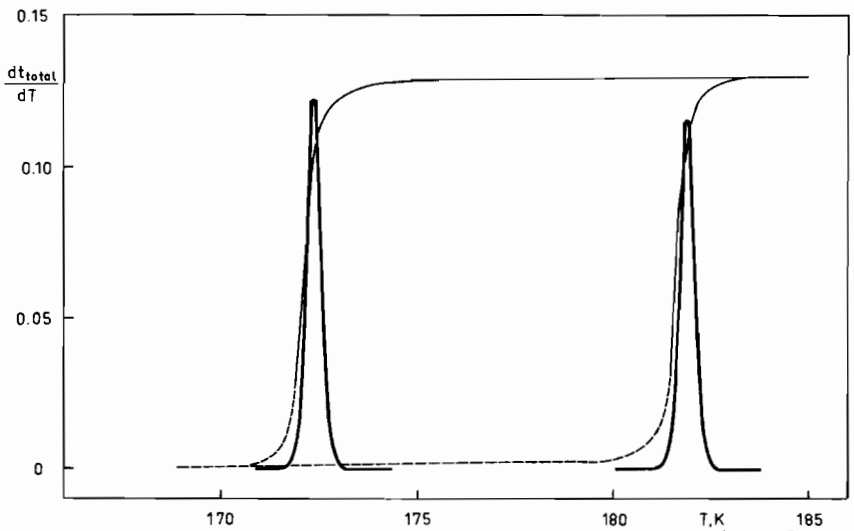

Fig. 4. Distribution functions p(T) and q(T) of transition temperatures $T(^1A_1 \rightarrow {}^5T_2)$ and $T(^5T_2 \rightarrow {}^1A_1)$ for individual domains in the neighborhood of $T_c^> = 181.86$ K and $T_c^< = 172.54$ K, respectively. Light curve is the experimental hysteresis loop corrected for the presence of additional modification (corrected part, broken curve).

atures T($^1A_1 \rightarrow {}^5T_2$) and T($^5T_2 \rightarrow {}^1A_1$) will be different from domain to domain. Thus T($^1A_1 \rightarrow {}^5T_2$) may be distributed among the domains according to some distribution function p(T) and similarly T($^5T_2 \rightarrow {}^1A_1$) according to q(T). The distribution functions may be determined, *e.g.* from the total effective thickness,

$$t_{total} = C[(1 - n_{s_{T_2}})f_{i_{A_1}} + n_{s_{T_2}} f_{s_{T_2}}] \quad (9)$$

where $C = \frac{1}{2}N\beta\, d\, \sigma_0$, and thus from the experimental data of the preceding section. For the main branches of the hysteresis loop of Fig. 2 one obtains

$$p(T) = \frac{d}{d\vec{T}}\, t_{total}$$
$$q(T) = \frac{d}{d\overleftarrow{T}}\, t_{total} \quad (10)$$

Application to the data of Table III produces the curves displayed in Fig. 4. Evidently, in the system studied here, the distribution functions for the two branches of the hysteresis loop are similar though not identical. As in the study by the Bragg and Williams type model above, the functions of Fig. 4 apply alone to the prominent part of the transition, the lower points in the hysteresis curve having been disregarded.

The domain model leads to several theorems [25] concerning relations between the distribution functions and the shape of the hysteresis curve and the scanning curves. Fig. 2 shows that only a single scanning curve is available at present. Upon close examination it becomes apparent that the descending curves will converge on the lower intersection point of the hysteresis loop rather than meet the descending boundary curve. This behaviour (*cf.* theorem 2 [25]) should indicate a wide distribution of domain properties. Due to the increased steepness of the boundary curve, the situation is less clear for the ascending curves, although the theorem seems to apply here as well. In addition, the slope of the scanning curves conforms to theorem 3 of the model [25]. It has been demonstrated [27] that theorems 3 and 4 of Everett [25] become invalid if interacting domains are considered. Although the criterion of theorem 4 is stronger than that of theorem 3, the applicability of theorem 3 to the present system indicates that, most likely, if any interactions between domains are effective, these should be small.

(iv) Temperature Dependence of Debye–Waller Factors

On the basis of ^{57}Fe Mössbauer spectra, Debye–Waller factors have been determined over the temperature range 12.2 to 302.0 K by application of the methods outlined in the experimental section. All measurements were performed for ascending temperatures. The results are listed in terms of $-\ln f_{i_{A_1}}$ and $-\ln f_{s_{T_2}}$ in Table I and Table II, respectively. In addition, the temperature dependence of both quantities is illustrated in Fig. 5.

From Fig. 5 it is evident that $-\ln f_{total}$ shows a discontinuity at the temperature $T_c^{\gtrless} = 181.9$ K of about 0.438 which corresponds to a decrease of $\Delta f_{total} = 35.4\%$ (*viz.* $f_{i_{A_1}} = 0.285$, $f_{s_{T_2}} = 0.184$ at 181.9 K). The change indicates a significant difference in the mean square amplitudes of certain lattice modes in the high-spin($^5T_2$) and low-spin($^1A_1$) phases which are specifically affected by the transition. This observation may be considered as supporting evidence for the first-order character of the phase transition associated with the high-spin($^5T_2$) $\rightleftharpoons$ low-spin($^1A_1$) conversion.

Above T_c, the values of $-\ln f_{s_{T_2}}$ may be well reproduced within the high-temperature approximation of the Debye model

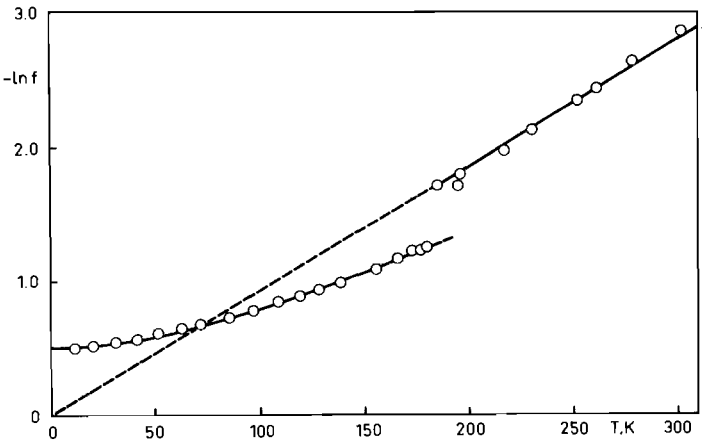

Fig. 5. Temperature dependence of Debye–Waller factors. The straight line represents a fit to $-\ln f_{s_{T_2}}$ within the high temperature approximation of the Debye model ($\Theta_{s_{T_2}} = 121$ K, $M_{s_{T_2}} = 57$ a.u.). The full curve in the low temperature region represents a fit to $-\ln f_{i_{A_1}}$ within the complete Debye model ($\Theta_{i_{A_1}} = 323$ K, $M_{i_{A_1}} = 12$ a.u.).

$$-\ln f_{(T \geq \Theta/2)} = \frac{3E_0^2}{Mc^2k\Theta}\left(\frac{T}{\Theta}\right) \quad (11)$$

In eqn. (11), E_0 is the γ-ray energy, Θ the Debye temperature and, for simple atomic lattices, M is the mass of the absorbing atom. Application of eqn. (11) to the data above T_c produces $\Theta_{^5T_2} = 121$ K if M is identified with the mass of the ^{57}Fe atom, $M_{^5T_2} = 57$ a.u. The fit is illustrated by the straight line in the upper part of Fig. 5.

Below T_c, the values of $-\ln f_{^1A_1}$ have been reproduced successfully only within the complete Debye model

$$f = \exp -\left\{\frac{3E_0^2}{Mc^2k\Theta}\left[\frac{1}{4}+\left(\frac{T}{\Theta}\right)^2\int_0^{\Theta/T}\frac{x\,dx}{e^x-1}\right]\right\} \quad (12)$$

the resulting parameter values being $\Theta_{^1A_1} = 323$ K and $M_{^1A_1} = 12$ a.u. The corresponding fit is illustrated by the full curve in the lower part of Fig. 5. Since in general $M_{^1A_1} > M_{^5T_2}$ would be expected, the obtained value of $M_{^1A_1}$ is unreasonable despite the excellent numerical agreement. For more details we refer to another recent study [17] where similar results were discussed in more detail.

(v) Temperature Dependence of X-Ray Diffraction

The temperature dependence of peak profiles of the X-ray diffraction was studied between 77 and 300 K as described in the experimental section. In general, the peak profiles observed in the low temperature, *i.e.* $^1A_1$, phase differed from those in the high temperature, *i.e.* $^5T_2$, phase. The change with temperature is exemplified in Fig. 6 for a particularly intense powder peak of $[Fe(bt)_2(NCS)_2]$ found in the diffraction angle range between $\theta = 4.90°$ and $\theta = 5.40°$. Thus between 148.0 and 182.0 K, a single line is found for a diffraction angle of, *e.g.* $\theta = 5.26°$ (corresponding spacing d = 8.42 Å). This line is assigned to the low-spin $^1A_1$ ground state on the basis of Mössbauer spectra obtained at the corresponding temperatures. At 185.2 K, a second, separate, powder peak is observed at $\theta = 5.17°$ (d = 8.56 Å) and similarly assigned to the high-spin $^5T_2$ ground state. It should be noted that the line at $\theta = 5.19°$ is discernible in Fig. 6 for temperatures between 182.5 and 185.2 K only. In a careful comparison of X-ray diffraction and Mössbauer effect data, this line correlates with the small step in $t_{^5T_2}/t_{total}$ between about 178 and 181 K (for increasing temperatures), *cf.* Fig. 2. Since it will be shown below that this protrusion is most likely due to a different modification of the compound, the line is excluded from the present analysis. For clarity of presentation, the diffraction lines for different temperatures though the same, *i.e.* $^1A_1$ or $^5T_2$, phase (*cf.* Fig. 6), have been connected each by a broken line.

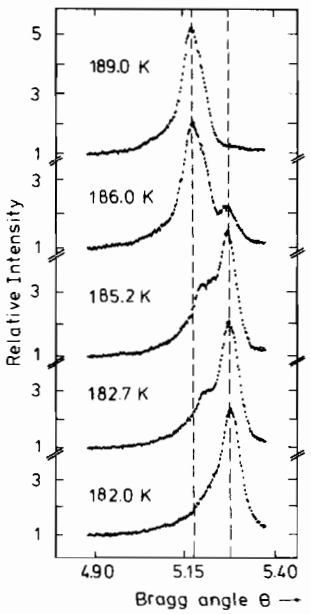

Fig. 6. Peak profiles of X-ray powder diffraction for $[Fe(bt)_2(NCS)_2]$ at the temperatures of 182.0, 182.7, 185.2, 186.0 and 189.0 K (T_c = 185.5 K). The diffraction peaks characteristic of the $^1A_1$ phase ($\theta = 5.26°$) and the $^5T_2$ phase ($\theta = 5.17°$) are connected by broken lines. The range covered extends from $\theta = 4.90°$ to $\theta = 5.40°$.

In order to obtain quantitative data from the analysis of the peak profiles, let us write the relative intensity for a single diffraction line as

$$I_{rel} = n_{^5T_2}\,V(F_{hkl}^{^5T_2})^2\,K(\theta) + (1 - n_{^5T_2})V(F_{hkl}^{^1A_1})^2\,K(\theta) \quad (13)$$

Here, V is the active volume of the specimen, $K(\theta)$ is an angular function containing the Lorenz and polarization factors, and the F_{hkl}^j, j = $^1A_1$ or $^5T_2$, are the structure factors for the $^1A_1$ or $^5T_2$ phase. The values of I_{rel} for the individual phases are obtained from a decomposition of the overall intensity pattern into Gaussians. If now, *e.g.*, $I_{^5T_2}/I_{total}$ is plotted *vs.* the temperature, V and $K(\theta)$ cancel out and the resulting effective intensities may be compared with the results of different physical measurements. On a qualitative basis then, the temperature dependence of $I_{^5T_2}/I_{total}$ is equivalent to that of $t_{^5T_2}/t_{total}$, *e.g.* for the increasing temperature branch of the hysteresis loop of Fig. 2. The results show, in addition, that the structure factors for the two phases, *i.e.* $F_{hkl}^{^5T_2}$ and $F_{hkl}^{^1A_1}$ are not much different.

(vi) ^{57}Fe Mössbauer Effect Measurements on Additional Samples of $[Fe(bt)_2(NCS)_2]$

In order to examine the reproducibility of the results reported above, two additional independently prepared samples of $[Fe(bt)_2(NCS)_2]$ have been

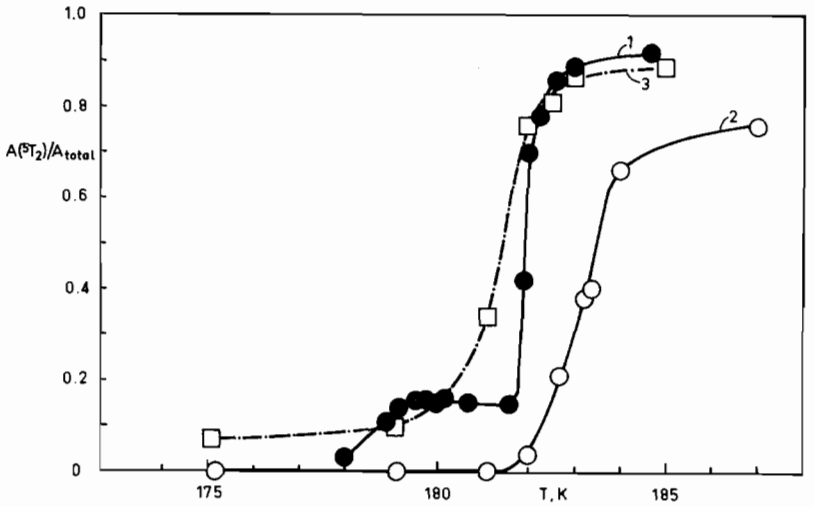

Fig. 7. Temperature dependence of the uncorrected area fractions $A(^5T_2)/A_{total}$ for three different samples of $[Fe(bt)_2(NCS)_2]$ in the neighborhood of $T_c^>$ ($T_c^>(1) = 181.86$ K, $T_c^>(2) \sim 183.5$ K, $T_c^>(3) \sim 181.5$ K).

investigated. It should be noted that the overall chemical and physical properties of these substances are identical to those of the first sample studied. Differences were found, however, for certain details of the phase transition which are of particular interest here. Figure 7 shows the uncorrected area functions $A(^5T_2)/A_{total}$ extracted from ^{57}Fe Mössbauer effect measurements in the neighborhood of $T_c^>$ (*i.e.* for increasing temperatures) for all three samples. It is evident that the detailed behaviour is different for any one sample, the transition temperatures being $T_c^>(2) \sim 183.5$ K and $T_c^>(3) \sim 181.5$ K, whereas $T_c^>(1) = 181.86$ K has been determined above. The even more important result is that samples no. 2 and no. 3 do not show the lower step in $t_{s_{T_2}}/t_{total}$ which is associated with the phase change in sample 1, *cf.* Fig. 2. This being the case we consider it most likely that this peculiarity is due to a small admixture, into sample 1, of another modification of $[Fe(bt)_2(NCS)_2]$ which may be characterized by $T_c^> \sim 178$ K. It is for this reason that this detail of the phase change in sample 1 has not been taken into account in the analyses of experimental data above.

It should be noted that differences in the detailed behaviour of high-spin($^5T_2$) $\rightleftharpoons$ low-spin($^1A_1$) transitions with temperature are not unusual. Such observations have been reported before for different preparations [1] as well as for well-defined different crystallographic modifications [28] of one and the same compound.

Discussion

Almost discontinuous high-spin($^5T_2$) $\rightleftharpoons$ low-spin($^1A_1$) transitions which are associated with hysteresis effects have been reported for several systems of the type discussed here, notably for $[Fe(4,7\text{-}(CH_3)_2\text{-phen})_2(NCS)_2]$ [7], $[Fe(paptH)_2](NO_3)_2$ [29], $[Fe(2\text{-pic})_3]Cl_2 \cdot H_2O$ [30], and $[Fe(phy)_2](ClO_4)_2$ [31]. Here, paptH = 2-(2-pyridylamino)-4-(2-pyridyl)-thiazole, 2-pic = 2-amino-methylpyridine, and phy = 1,10-phenanthroline-2-carbaldehyde phenylhydrazone. The only more detailed study available, *i.e.* on $[Fe(4,7\text{-}(CH_3)_2\text{-phen})_2(NCS)_2]$ [7], shows that in this system the high-spin($^5T_2$) $\rightleftharpoons$ low-spin($^1A_1$) transition is centred for increasing temperatures on $T_c^>$ = 121.5 K, whereas for decreasing temperatures $T_c^<$ = 118.6 K. The hysteresis thus amounts to $\Delta T_c = 3.1$ K as compared to $\Delta T_c = 9.5$ K in the present case. A detailed analysis of the $t_{s_{T_2}}/t_{total}$ data using a Bragg and Williams type model [20, 21] produced agreement, at least on a qualitative basis, for $\Delta S = 50$ to 70 J K^{-1} mol^{-1} and $\Gamma = 192$ to 199 cm^{-1}. These values are of reasonable magnitude as are those obtained for the present system, *cf.* $\Delta S = 50$ to 100 J K^{-1} mol^{-1} and $\Gamma = 310$ to 350 cm^{-1}. In addition, both sets of data are consistent with the condition $\Gamma/k \geqslant 243$ K which is required in order to observe a jump between quantities characterizing the two states [20]. On the other hand, it has been realized that the differences between observed and computed values are typical for models of the type employed [22]. Similar discrepancies are again found in the system studied at present, *cf.* Fig. 3. The model is also not capable of reproducing scanning curves like the one in Fig. 2, since only discontinuous changes in $n_{s_{T_2}}$ are formed.

The application of the domain model provides additional insight into the possible mechanism of high-spin($^5T_2$) $\rightleftharpoons$ low-spin($^1A_1$) transitions in solids. The results obtained above indicate that the assumption of domain formation by both $^1A_1$ and $^5T_2$ molecules is not unfounded, and that any interactions between these domains are likely to be small. More

detailed information could be obtained from the analysis of multiple scanning curves applying the theorems of Everett [25]. However, the required accurate experimental data are not easy to accumulate, particularly not for sample 1 of $[Fe(bt)_2(NCS)_2]$, on which the present study was almost exclusively based. The complications associated with this sample are apparent from Fig. 2 and from the data in Results section (vi).

An experimental, and thus more conclusive, evidence for the formation of domains in $[Fe(bt)_2(NCS)_2]$ emerges from the investigation of the peak profiles of X-ray diffraction. The observation that the quantities $t_{^5T_2}/t_{total}$ and $I_{^5T_2}/I_{total}$ from ^{57}Fe Mössbauer effect and X-ray data, respectively, show equivalent temperature dependences is of considerable significance. It is obvious that Mössbauer effect data are characteristic for the molecular, X-ray data for the crystal properties. The above result will then be obtained only if crystal domains of finite dimension exist for both the $^1A_1$ and $^5T_2$ ground state molecules which are capable of producing the observed X-ray diffraction. Consequently, the high-spin($^5T_2$) $\rightleftharpoons$ low-spin($^1A_1$) transition in solids proceeds, at least in the system $[Fe(bt)_2(NCS)_2]$, by way of the formation of domains rather than that of isolated, *i.e.* statistically distributed, molecules in the two ground states, $^1A_1$ and $^5T_2$. It should be noted that this process is thermodynamically prefered to one where a large number of separated molecules in the resulting ground state is formed as a consequence of the transformation $^1A_1 \rightarrow {}^5T_2$ or *vice versa*.

A discontinuity of the Debye–Waller factor of $\Delta f_{total} \sim 20\%$ has been observed before [8] at the high-spin($^5T_2$) $\rightleftharpoons$ low-spin($^1A_1$) transition in $[Fe(4,7\text{-}(CH_3)_2\text{-phen})_2(NCS)_2]$ ($f_{^1A_1} = 0.413$, $f_{^5T_2} = 0.342$, both at $T_c = 121.5$ K). This result may be compared with that of $\Delta f_{total} \sim 35.4\%$ obtained for $[Fe(bt)_2(NCS)_2]$ in this study. It should be noted that the Debye–Waller factor provides a collective representation of lattice dynamics. A discontinuity in the total Debye–Waller factor may thus be considered as evidence for a phase transformation, although more detailed conclusions are difficult to achieve. In $[Fe(bt)_2(NCS)_2]$, this conclusion adds weight to the similar evidence derived from the almost discontinuous change of magnetic properties [13] and of the relative effective thickness, $t_{^5T_2}/t_{total}$, of the Mössbauer effect. In addition, the observation of hysteresis is likewise an indication of a phase change. The most conclusive evidence for a phase transformation is, however, the finding of separate X-ray diffraction peaks for the $^1A_1$ and the $^5T_2$ ground state molecules and the fact that the quantity $I_{^5T_2}/I_{total}$ shows an almost discontinuous behaviour at T_c which is moreover equivalent to that of $t_{^5T_2}/t_{total}$.

With regard to the hysteresis argument above, we may be confronted with the fact that the transition in $[Fe(paptH)_2](NO_3)_2$ shows quasi-continuous behaviour despite the observed hysteresis [29]. However, in solids, the continuous character of an internal dependent variable, *viz.* $t_{^5T_2}/t_{total}$, as function of, *e.g.* the temperature, is no guarantee for an equilibrium process, although the converse is in general true.

An attempt may be made to classify the transition in $[Fe(bt)_2(NCS)_2]$ on the basis of available evidence. According to the conventional *thermodynamic* classification, a transition of first order is characterized, by definition, by a discontinuous change of energy, *i.e.* a latent heat, and discontinuities in volume and in lattice parameters. Also, the transition takes place sharply at a particular temperature. In the case of $[Fe(bt)_2(NCS)_2]$, a discontinuous change of lattice parameters and thus volume may be inferred from the behaviour of X-ray diffraction peaks (*cf.* Results section (v) and the Debye–Waller factor (*cf.* Results section (iv). A latent heat as well as a change in entropy are required in order to interpret the Mössbauer effect data by a Bragg and Williams type model (*cf.* Results section (iii). On a thermodynamic basis, the transition may thus be considered as of *first order*, although Fig. 2 shows that the first-order character is 'smeared out', particularly towards the high-temperature side of the transition. The origin of this complication are usually local nonuniformities and stresses due to various defects within or to grain boundaries between crystals.

Another accepted classification scheme is essentially *geometrical* [32].. Based on the general character of a high-spin $\rightleftharpoons$ low-spin transition [2–4], no breaking of bonds or any other major changes of molecular constituents are expected. This assumption is in agreement with all available structure data for spin transformations [9–12]. The recent observation of molecular dynamics in solid iron(III) tetraphenylporphinatobenzenethiolate benzenethiol [33] seems to be rather exceptional. In addition, all observed changes are *reversible*, even in a single crystal. Consequently, the observed transformation may be termed a *pure displacive* transition. It should be noted that, in reversible transitions, the size of the discontinuity is not obviously correlated with the underlying mechanism of the transition [32]. Therefore, if this classification is adopted, the details of the discontinuities observed for any particular physical property as well as its size are important additional characteristics.

Acknowledgements

The authors appreciate financial support by the Deutsche Forschungsgemeinschaft and the Fonds der Chemischen Industrie.

References

1 E. König and K. Madeja, *Inorg. Chem., 6,* 48 (1967).
2 E. König, *Ber. Bunsenges. Phys. Chem., 76,* 975 (1972).
3 E. König and G. Ritter, *Mössbauer Effect Methodology, 9,* 1 (1974).
4 H. A. Goodwin, *Coord. Chem. Rev., 18,* 293 (1976).
5 M. Sorai and S. Seki, *J. Phys. Chem. Solids, 35,* 555 (1974).
6 J. Frenkel, in 'Kinetic Theory of Liquids', Oxford University Press (1947).
7 E. König and G. Ritter, *Solid State Commun., 18,* 279 (1976).
8 E. König, G. Ritter and B. Kanellakopulos, *J. Phys. C, 7,* 2681 (1974).
9 E. König and K. J. Watson, *Chem. Phys. Lett., 6,* 457 (1970).
10 M. A. Hoselton, L. J. Wilson and R. S. Drago, *J. Am. Chem. Soc., 97,* 1722 (1975).
11 L. G. Leipoldt and P. Coppens, *Inorg. Chem., 12,* 2269 (1973).
12 D. Gatteschi, C. A. Ghilardi, A. Orlandini and L. Sacconi, *Inorg. Chem., 17,* 3023 (1978).
13 G. Bradley, V. McKee, S. M. Nelson and J. Nelson, *J. Chem. Soc. Dalton,* 522 (1978).
14 G. A. Bykov and Pham Zuy Hien, *Zhur. Eksp. Teor. Fiz., 43,* 909 (1962).
15 G. Lang, *Nucl. Instr. Meth., 24,* 425 (1963).
16 E. König, G. Ritter and H. A. Goodwin, *Chem. Phys., 5,* 211 (1974).
17 E. König, G. Ritter, W. Irler, H. A. Goodwin and B. Kanellakopulos, *J. Phys. Chem. Solids, 39,* 521 (1978).
18 E. König, G. Ritter, W. Irler and B. Kanellakopulos, *J. Phys. C, 10,* 603 (1977).
19 B. Kanellakopulos, E. König, G. Ritter and W. Irler, *J. Phys. (Paris) Suppl., 37,* C6-459 (1976).
20 C. P. Slichter and H. G. Drickamer, *J. Chem. Phys., 56,* 2142 (1972).
21 H. G. Drickamer and C. W. Frank, 'Electronic Transitions and the High Pressure Chemistry and Physics of Solids', Chapman and Hall, London (1973).
22 E. A. Guggenheim, 'Mixtures', Oxford University Press (1952).
23 H. E. Stanley, 'Introduction to Phase Transitions and Critical Phenomena', Oxford University Press (1971).
24 D. H. Everett and W. I. Whitton, *Trans. Faraday Soc., 48,* 749 (1952).
25 D. H. Everett and F. W. Smith, *Trans. Faraday Soc., 50,* 187 (1954).
26 D. H. Everett, *Trans. Faraday Soc., 50,* 1077 (1954); *ibid., 51,* 1551 (1955).
27 J. A. Enderby, *Trans. Faraday Soc., 52,* 106 (1955).
28 E. König, K. Madeja and K. J. Watson, *J. Am. Chem. Soc., 90,* 1146 (1968).
29 G. Ritter, E. König, W. Irler and H. A. Goodwin, *Inorg. Chem., 17,* 224 (1978).
30 M. Sorai, J. Ensling, K. M. Hasselbach and P. Gütlich, *Chem. Phys., 20,* 197 (1977).
31 E. König, G. Ritter, W. Irler and H. A. Goodwin, to be published.
32 H. D. Megaw, 'Crystal Structures, A Working Approach', W. B. Saunders, Philadelphia (1973).
33 J. P. Collman, T. N. Sorrell, K. D. Hodgson, A. K. Kulshrestha and C. E. Strouse, *J. Am. Chem. Soc., 99,* 5180 (1977).